IOP Conference Series: Materials Science and Engineering

PAPER • **OPEN ACCESS**

A study on stabilizing mechanism of flap countermeasures mitigating VIV of a box girder bridge section

To cite this article: Phan Duc Tam *et al* 2023 *IOP Conf. Ser.: Mater. Sci. Eng.* **1289** 012008

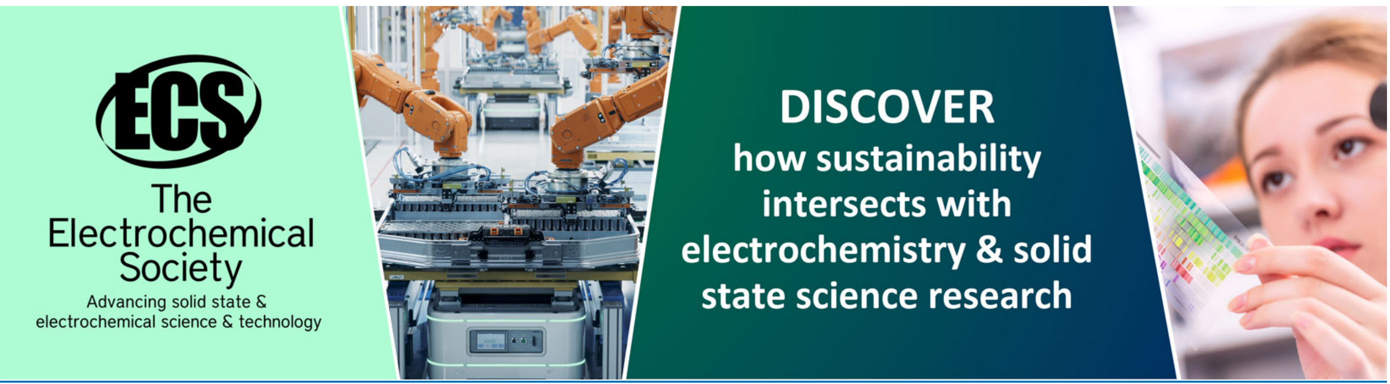

A study on stabilizing mechanism of flap countermeasures mitigating VIV of a box girder bridge section

Phan Duc Tam[1,2], Hiroshi Katsuchi[1,*], Wang Jiaqi[1], Hiroshi Tamura[1], Kensho Hirao[1]

[1] Department of Civil Engineering, Yokohama National University; Yokohama 240-8501, Japan
[2] Faculty of Bridge and Road Engineering, The University of Danang – University of Science and Technology; Danang 550000, Vietnam

[*] Corresponding author's e-mail: katsuchi@ynu.ac.jp

Abstract. As bridge spans stretch, the structure becomes more flexible and susceptible to dynamic wind effects causing harmful wind-induced vibration. The biggest issue with the design of long-span bridges is the possibility of vibration caused by vortices. This study examines the mechanism of the decrease in the amplitude of vortex-induced vibration for the box girder using a flap countermeasure. Aerodynamic countermeasures such as a flap have successfully increased bridge deck aerodynamic stability. However, their stabilizing mechanism has yet to be fully understood. Based on the proposed approach, a wind tunnel experiment and a CFD technique are used to investigate the aerodynamic instability of the bridge girder in the presence of aerodynamic countermeasures. The flow fields surrounding the bridge deck, both with and without the flap, are examined, and the experiment outcomes are compared. Flow imagery is utilized to explain and understand the modified flow properties surrounding the bridge girder in the presence of aerodynamic countermeasures that minimize vibration amplitude. Indeed, installing flaps on a girder leads to increased turbulence over the surface and at the leeward side, which disrupts vortex formation and decreases lift forces on the structure. In addition, the results revealed that the efficiency of the flap is related to the installed location of the flap and the flap length. This research provides a reliable framework for designing the flap countermeasure and significantly improves the aerodynamic stability of a deck-flap system.

1. Introduction

The influence of wind forces, which may create self-excited vibrations that may lead to structural collapse, is one of the major issues associated with constructing long-span bridges. Long-span bridges have commonly utilized box girders, which are highly flexible and have low damping, making them susceptible to aerodynamic instability and vibration caused by wind. The vortex-induced vibration phenomenon was observed in typical cases such as the Shin Minato and Trans-Tokyo Bay bridges [1].

Therefore, aerodynamic countermeasures have been developed to mitigate these effects and make bridge girders more aerodynamically stable, thereby enhancing the safety and longevity of bridges. Box girders with a small width-to-depth ratio can benefit from adding various attachments to improve their stability against vortex-induced vibrations (VIV) and flutter. Improved aerodynamic stability may be achieved by modifying the flow at the girder's leading edge using flaps, fairings, wind noses, deflectors, and spoilers.

One of the most successful defenses against VIV for bridge girders is a countermeasure known as the flap. In the case of the Meiko Nishi bridge, flaps were found to be a suitable measure for preventing vortex-induced vibration [2]. This idea was further developed in subsequent studies into solutions for controlling VIV. The Trans-Tokyo Bay Bridge was tested with fairings, double flaps, and skirts to assess their effectiveness in mitigating wind-induced vibration [3].

Generally, wind tunnel experiments are conducted to investigate the aeroelastic behavior of a long-span bridge girder section with various types of countermeasures at different wind angles of attack and various wind speeds to select the best wind resistance from the results. In the case of the Shin Minato bridge, which experienced vortex-induced vibration, an investigation was conducted to identify potential aerodynamic countermeasures to address the problem. Katsuchi [4] conducted wind tunnel tests and found that adding a flap to the bridge's girder section effectively reduced the amplitude of the vibrations. This determination was based on comparing the behavior of the actual bridge with that of the bridge girder section tested in their experiments. However, the mechanism of vibration regulation is unknown, and this is a gap in the experimental research. Therefore, CFD (Computational Fluid Dynamics) technique and Particle Image Velocimetry (PIV) experiments were performed to clarify and comprehend the changes in the flow structures surrounding the bridge girder, both with and without the flap measures.

Particle Image Velocimetry tests of the flow field around bridge girders in wind tunnels are a valuable tool for understanding the aerodynamics of bridges and the effect of flap countermeasures on the stability of these structures. PIV provides a high-resolution, non-intrusive measurement of the fluid flow, allowing researchers to see how the flow interacts with the structure and how flap countermeasures affect the flow. The results of PIV tests provide valuable information to optimize the design and configuration of flap countermeasures and boost bridges' aerodynamic stability. The aerodynamic strength of a twin-box girder using PIV was performed [5], [6]. Furthermore, PIV measurements were taken to examine the box girder's flutter performance [7].

In addition, the potent instrument of Computational Fluid Dynamics is used to simulate and analyze the behavior of fluids, such as wind engineering. CFD simulations can generate detailed information about the flow fields' pressure, velocity, and turbulence around the bridge. This information is valuable in gaining a comprehensive understanding of the complex flow patterns that occur around the bridge girders. An example of a CFD application to wind analysis on a bridge girder is examining the impact of a flap on the wind flow over a box girder section. The Reynolds-Averaged Navier-Stokes (URANS) method and a k-omega turbulence model were used in this study [8].

The main objective of this study is to elucidate and comprehend the mechanisms responsible for stabilizing box girder sections in the presence of flap measures. Particle Image Velocimetry measurements were utilized to visualize the flow structures in three different areas: the local gap, the whole flow field, and the leeward side of the box girder. Aerodynamic coefficients and flow fields surrounding the bridge girder were analyzed using computational fluid dynamics analysis, which included both static and dynamic simulations. Based on the results obtained from PIV tests and CFD simulation, the influence of flap measures on aerodynamic stability can be analyzed by examining the flow structures around the bridge girder. The results of this research will help to a better knowledge of the aerodynamic behavior of box girder bridges, especially with regard to the influence that flap measures have on the stability of these structures.

2. Wind tunnel test

2.1. Aeroelastic response measurements

A wind tunnel experiment was performed at Yokohama National University to determine an effective countermeasure for controlling the Vortex-Induced Vibration (VIV) in the girder section of the Shin Minato bridge. The test was carried out in a Closed-Circuit Wind Tunnel constructed in 1993, which

IOP Conf. Series: Materials Science and Engineering 1289 (2023) 012008 doi:10.1088/1757-899X/1289/1/012008

can generate wind speeds of up to 40m/s. The cross-sectional size of the wind tunnel is shown in Figure 1 to be 1.8m x 1.8m.

The experiment was undertaken using the procedure outlined in Figure 2. The model was suspended from the top and bottom using springs, which enabled vertical and torsional vibrations to reproduce. An electromagnetic damper adjusted the damping value to a predetermined level. Additionally, a laser displacement meter was utilized to measure the vibration displacement of the model without physical contact.

Figure 1. Closed-Circuit Wind Tunnel at Yokohama National University.

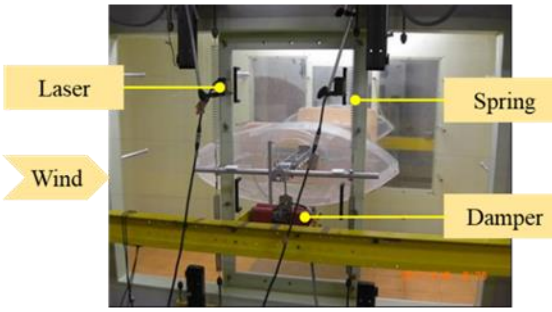

Figure 2. Installation of the wind tunnel test.

Table 1. Test condition.

Parameter	Unit	Full-Scale	Model
Width (*B*)	m	15	0.30
Height (*D*)	m	4.5	0.09
Scale		-	1/50
Equivalent mass (*m*)	(kg/m)	12.15 x 10^3	4.8810
Vertical frequency	Hz	0.464	2.7180
Torsional frequency	Hz	1.208	6.2550
Structural damping: Vertical			0.0139
Structural damping: Torsion			0.0164

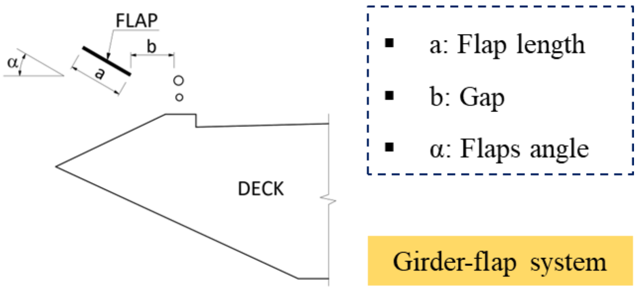

Figure 3. Flap parameters.

Table 1 presents the comparable parameters between the actual bridge specifications and the wind tunnel experiments. The partial model was scaled down to 1/50, corresponding to the design scale, accounting for the wind tunnel dimensions and the model size during the design phase.

As depicted in Figure 3, the properties of the flap are influenced by three parameters: flap length, angle, and the gap between the flap and bridge girder. Figure 4 indicates a box girder without a flap, whereas Figure 5 displays the same design but with a flap attached.

Figure 4. No-Flap.

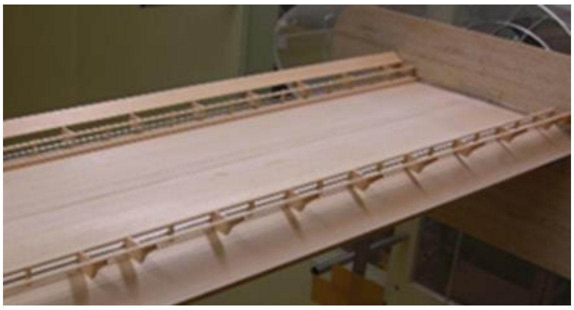

Figure 5. Flaps.

2.2. Particle Image Velocimetry (PIV) measurements

Figure 6 shows how flaps for bridge girders have been made using 3D printing. After the printing procedure, the deck-flap system used for PIV testing is assembled by attaching the flap to the bridge girder. The laser is positioned at the top of the wind tunnel for the gap flow and entire flow tests, while it is positioned downstream to measure the wake flow behavior. Figure 7 illustrates the principle of PIV measurements.

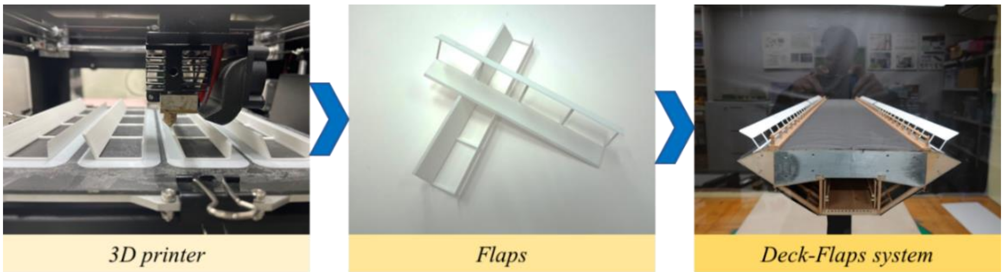

Figure 6. Flaps generation.

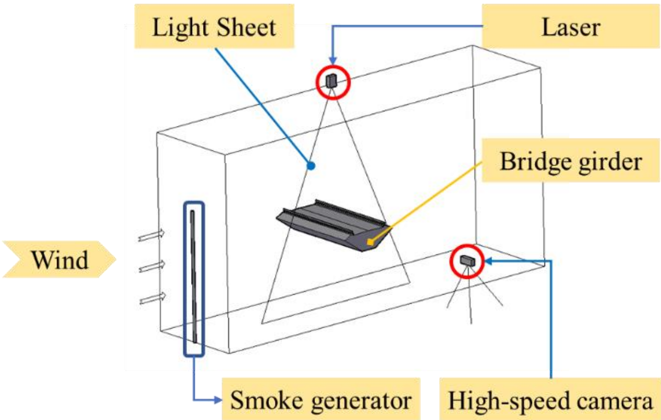

Figure 7. Principle of PIV.

3. Numerical simulation

3.1. Static simulation

3.1.1. Governing equation. The fluid domain is governed by the filtered Navier-Stokes equations for incompressible flow with a constant density [9], [10]:

$$\frac{\partial \rho \overline{u_i}}{\partial x_i} = 0;\ \frac{\partial}{\partial t}(\rho \overline{u_i}) + \frac{\partial}{\partial x_j}\left(\rho \overline{u_i u_j}\right) = \frac{\partial}{\partial x_j}\left(\mu \frac{\partial \overline{u_i}}{\partial x_j}\right) - \frac{\partial \overline{p}}{x_i} - \frac{\partial \tau_{ij}}{\partial x_j} \tag{1}$$

where $\overline{u_i}$, $\overline{u_j}$ are the averaged velocities; u_i', u_j' are the fluctuating velocity; $\overline{p}$, ρ are the time-averaged pressure and the flow density, respectively; $\rho\overline{u_i' u_j'}$ is known as the Reynolds stresses; $\partial\overline{\tau_{ij}}$ is the time-averaged viscous stress tensor component and can be articulated as:

$$\partial\overline{\tau_{ij}} = \mu\left(\frac{\partial \overline{u_i}}{\partial x_j} + \frac{\partial \overline{u_j}}{\partial x_i}\right) \tag{2}$$

Reynolds stresses $\rho\overline{u_i' u_j'}$ is computed as follows:

$$\rho\overline{u_i' u_j'} = \mu_t\left(\frac{\partial \overline{u_i}}{\partial x_j} + \frac{\partial \overline{u_j}}{\partial x_i}\right) - \frac{2}{3}\rho\delta_{ij}k \tag{3}$$

where μ is the dynamic viscosity, while δ_{ij} is Kronecker's delta; μ_t is eddy viscosity; *k* is the turbulent kinetic energy.

The k-Omega Shear Stress Transport (k-ω SST) turbulence model, initially suggested by Menter [11] and commonly utilized in aerodynamics, is employed in the simulation. This model is a hybrid that combines the Wilcox k-Omega model and the k-Epsilon model, both of which are two-equation eddy-viscosity models. It is classified as part of the Reynolds-averaged Navier-Stokes (RANS) turbulence model family.

3.1.2. Aerodynamic coefficients. The formula of drag, lift, and moment coefficient could be written by following:

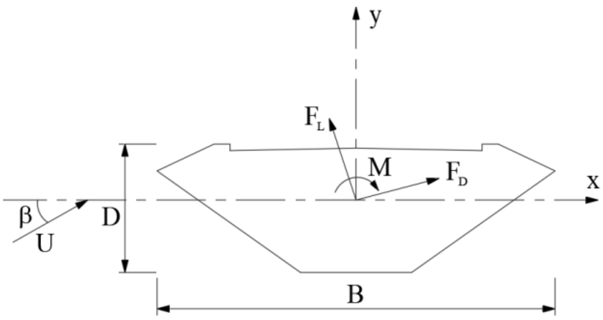

Figure 8. Definition of direction forces and angle of attack.

$$C_D = \frac{F_D}{\frac{1}{2}\rho U^2 D} \tag{4}$$

$$C_L = \frac{F_L}{\frac{1}{2}\rho U^2 B} \tag{5}$$

$$C_M = \frac{M}{\frac{1}{2}\rho U^2 B^2} \tag{6}$$

where F_D and F_L are the drag and lift forces, C_D and C_L are Drag and Lift coefficients, respectively. *U* is uniform oncoming velocity; *B* and *D* are the representative dimensions of the object.

Force coefficients are the essential criteria to characterize flow behavior. Figure 8 shows a fixed object set and then put through a wind load to clarify the formulas. With the idea that the motion is very slow and using the quasi-steady theory, the aerodynamic force acting on a stable object can be normalized as the force.

3.1.3. Domain and boundary condition. In order to study the extent of influence of fluid flow around the bridge girder section, the girder section is inserted into a computational domain with dimensions of 40 times the section's characteristic dimension (*D*) in width and 20 times *D* in height. The boundary conditions are a velocity inlet and a pressure outlet, representing the inlet and outlet. No-slip condition is assigned at the bridge girder section, while symmetry is imposed at the top and bottom. The computational domain, as well as the boundary conditions, are broken out in depth in Figure 9.

Generating a mesh for a bridge girder is crucial in conducting computational fluid dynamics analysis. A high-quality mesh with appropriate nodes and cells is necessary for accurate and detailed simulation. This study utilized a structured mesh known for its high quality and accuracy. Figure 10 shows the fine mesh near the bridge girder sections.

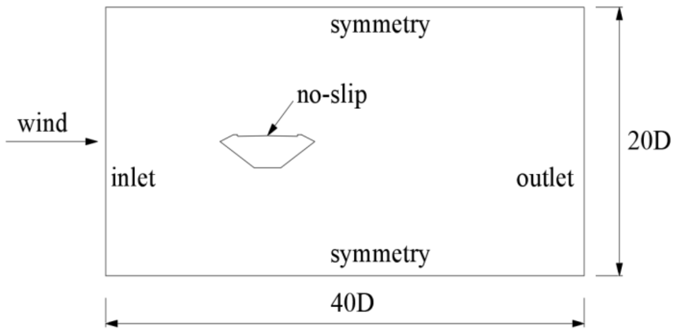

Figure 9. Domain and boundary condition.

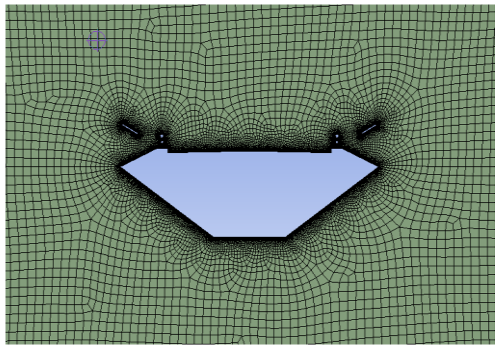

Figure 10. Meshing.

3.2. Dynamic simulation

According to Scanlan and Tomko (1971), [12] aerodynamic derivatives derived the following Equation to represent the self-excited aerodynamic forces operating on an oscillating bluff body H_i^*, A_i^* (i=1~4):

$$L_h = \frac{1}{2}\rho U^2 B\left[KH_1^*(K)\frac{\dot{h}}{U} + KH_2^*(K)B\frac{\dot{\alpha}}{U} + K^2H_3^*(K)\alpha + K^2H_4^*\frac{h}{B}\right] \tag{7}$$

$$M_\alpha = \frac{1}{2}\rho U^2 B^2\left[KA_1^*(K)\frac{\dot{h}}{U} + KA_2^*(K)B\frac{\dot{\alpha}}{U} + K^2A_3^*(K)\alpha + K^2A_4^*\frac{h}{B}\right]$$

where L_h is the self-excited lift force; M_α is the self-excited pitching moment; h and α are vertical and torsional displacement, respectively; B is the length of body width; U is uniform velocity, and K is reduced frequency.

Aerodynamic derivatives are commonly employed in the analysis of coupled flutter in practice. This study considers a model subjected to vertical 1DOF (degree of freedom) sinusoidal vibration. The mathematical representation of the model's displacement and unstable lift force might take the following form:

$$h = h_o \sin(\omega t) \tag{8}$$

$$L_h(t) = L_o \sin(\omega t + \Phi) \tag{9}$$

where h_0 is the amplitude of displacement, Φ is the phase lag between unstable lift force and vertical translation, and the amplitude of the lift force acting on the vertical 1DOF sinusoidal vibration is denoted by L_0.

For the vertical 1DOF vibration, the unsteady lift force (7) can be written:

$$L_h = \frac{1}{2}\rho U^2 B\left[KH_1^*(K)\frac{\dot{h}}{U} + K^2H_4^*\frac{h}{B}\right] \tag{10}$$

By summarizing Equations (8), (9), and (10), the flutter derivative H_1^* can be obtained based on the following formula:

$$H_1^* = -\frac{L_o Sin\Phi}{\rho B^2\omega^2 h_o} \tag{11}$$

4. Results and discussions

4.1. Wind tunnel test collection

As seen in Figure 11, a vertical bending vortex on the actual bridge caused vibration with a maximum amplitude of 35 cm. Figure 12 depicts the results of an experiment performed in a wind tunnel at a scale of 1/50, in which a vertical deflection vortex-induced vibration of 40.3 cm occurred at an angle of attack of 0 degrees. The vortex-induced vibration occurred at the incoming wind speed ranging from 11 m/s to 13 m/s. Figure 13 illustrates the maximum amplitude of torsional vortex excitation at 0 degrees of attack as 1.2 degrees. As a result, many types of flaps were included in the test in order to investigate the potential options for dampening the oscillations.

Flaps' impact on wind flows at Shin Minato Bridge's cross-section was studied in a wind tunnel. According to the results, the area without a flap had the maximum vibration amplitude (40,3 cm), whereas the presence of flaps resulted in a drop in amplitude. The amplitude decrease was different depending on the geometry of the flap. For example, when the flap length (a) is 1m, and the flap angle (α) is 10 degrees, an increase in the flap distance decreases the vertical deflection, as illustrated in Figure 14. Figure 15 shows some cases with the same flap length of 1m and angle of 30 degrees, where an increase in the flap distance led to a decrease in vertical displacement.

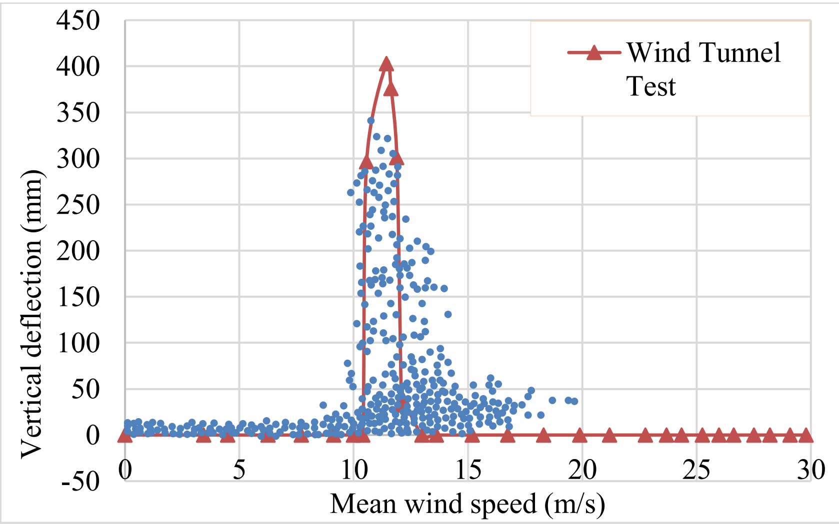

Figure 11. Vertical amplitude (Actual bridge) [4].

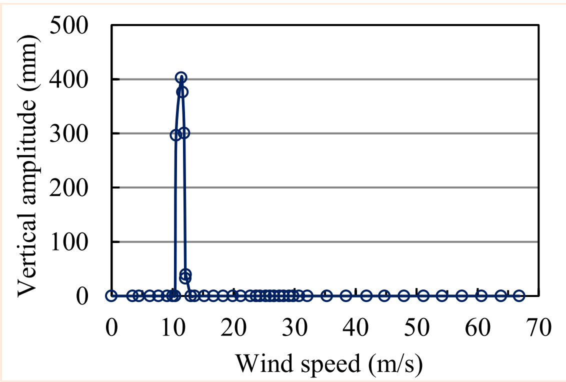

Figure 12. Vertical amplitude – No flap (WTT).

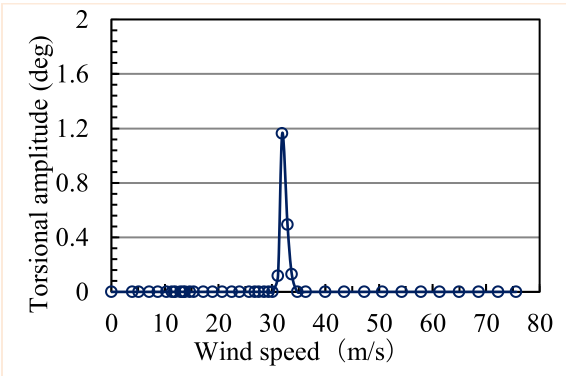

Figure 13. Torsional amplitude – No flap (WTT).

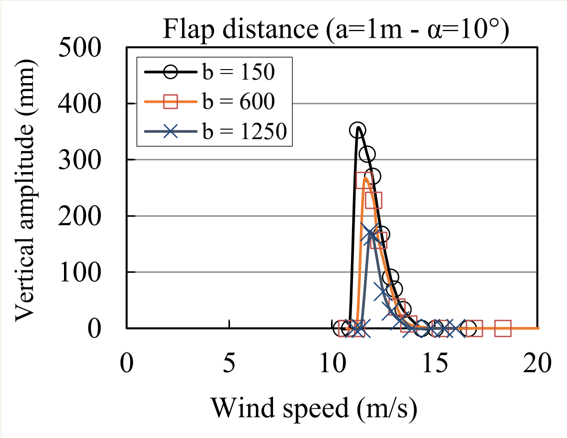

Figure 14. Vertical amplitude (a=1 and α=10°).

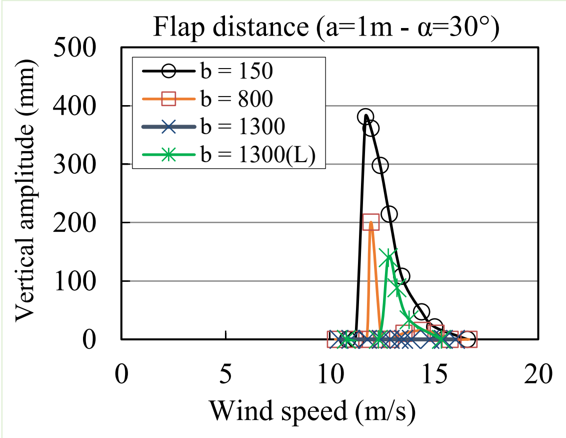

Figure 15. Vertical amplitude (a=1 and α=30°).

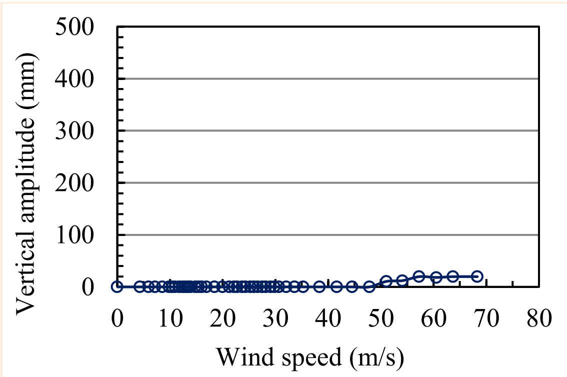

Figure 16. Vertical amplitude S30-1-1.3 (WTT).

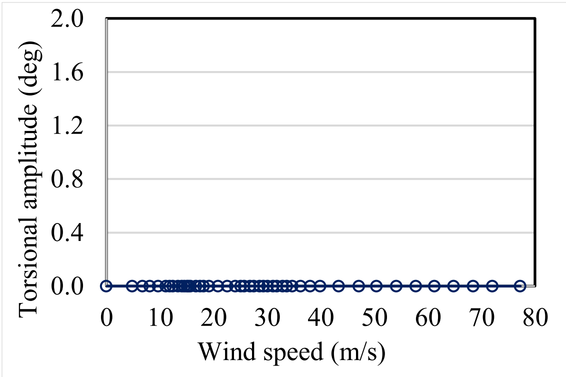

Figure 17. Torsional amplitude S30-1-1.3 (WTT).

Moreover, vortex-induced oscillation, such as in the S30-1-1.3 case, no longer appeared. The flap with a 30-degree angle and a large gap was the most effective at mitigating vibration. Based on the results above, it was determined that the flap configuration labeled as S30-1-1.3, with a length (a) of 1.0 m, flap angle (α) of 30 degrees, and flap distance (b) of 1.3 m from the handrail exhibited the best wind resistance. The effectiveness of the flap configuration in reducing the amplitude of vortex-induced oscillation was demonstrated in Figure 16 and Figure 17.

4.2. PIV test

In order to provide a conservative conclusion, PIV tests were conducted in a wind tunnel with a uniform incoming flow. It should be noted that the maximum vertical translation of the bridge girder occurs when wind speed approaches the reduced velocity. Therefore, to account for this, the uniform velocity used in the PIV tests was set to the reduced velocity of 2, as indicated by the results of aeroelastic measurements.

4.2.1. The local flow measurements. Figures 18 and 19 demonstrate that two high-speed cameras were used to capture images of flow fields in the local area around the flaps. The results show that vortices are formed above the deck surface in the case of the bridge girder without flaps. However, no clear vortices were observed in cases where flaps were installed. Furthermore, the direction of the vortices at the trailing edge was clockwise in the bridge girder section case, while the reverse direction was observed in the flap cases.

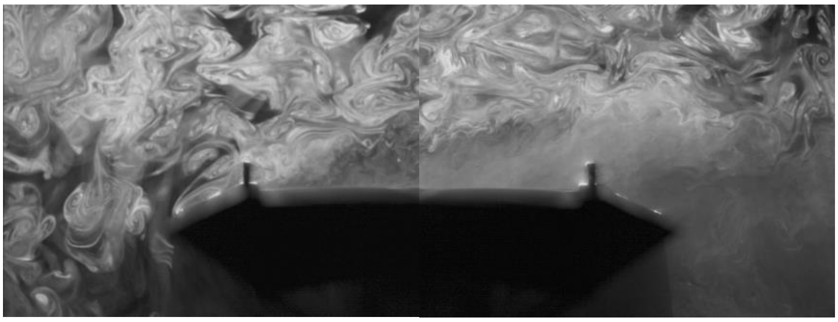

Figure 18. Local flow measurements – No flaps case.

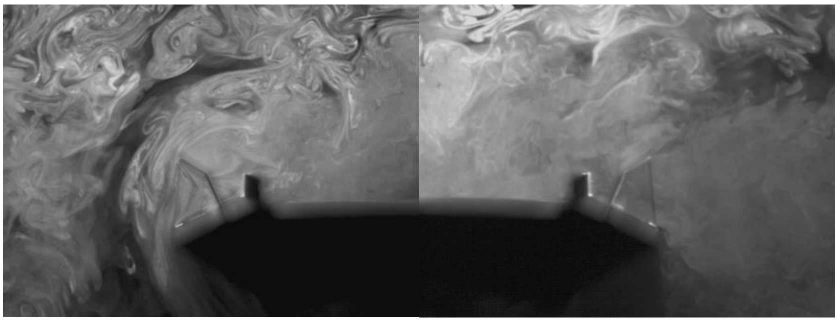

Figure 19. Local flow measurements – S30-1-1.3 case.

4.2.2. The entire flow field test. Several PIV tests were conducted to investigate the velocity fields of the entire flow region. A more profound comprehension of the VIV mechanism of closed-box girders with diverse geometrical flap configurations was achieved by detecting a tracer's motion trajectory and velocity in the flow region. Figures 20 and 21 show the flow fields above the bridge girder without and with flaps. In particular, the small vortexes could be neglected above the surface bridge girder in the no-flap case. However, the presence of flaps prevented the occurrence of a comparable phenomenon.

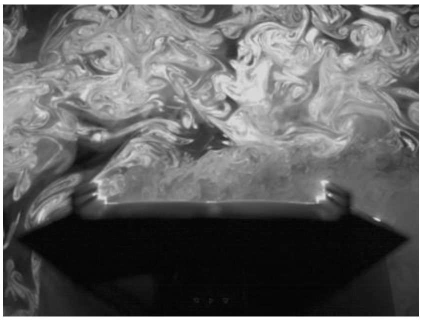

Figure 20. Whole flow fields – No flaps case.

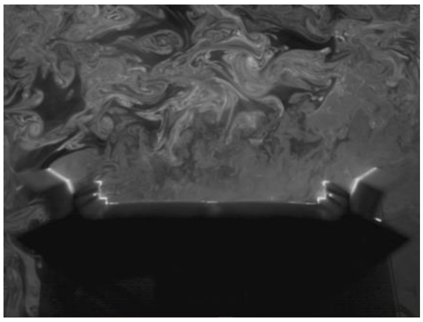

Figure 21. Whole flow fields – S30-1-1.3 case.

4.2.3. Downstream test. As one of the critical characteristics of vortices, in order to investigate the effect of vortex patterns on the VIV performance of closed-box girders with various geometrical configurations, the vorticity around the wake regions was compared as an essential characteristic of vortices. Figures 22 and 23 depict the instantaneous vorticity distributions, primarily around the downstream areas of the closed-box girders. Figure 22 shows the presence of large vortices behind the deck in the no-flap case, whereas in the flap case (especially the S30-1-1.3 case) shown in Figure 23, the presence of such vortices is not as clear.

The flow correlation around the bridge girder may be influenced by the variation in vortex structures observed on the downwind side for different flap configurations. The modification of wind-induced forces caused by this phenomenon has the potential to alter the aerodynamic performance of the bridge.

Figure 22. Downstream flow fields test: Case No flaps (SNF).

Figure 23. Downstream flow fields test: Case S30-1-1.3.

4.3. Numerical validation
In this section, the accuracy of the numerical simulations was confirmed by comparing the results obtained from the simulations with those obtained from wind tunnel tests (WTT). The mean values of important aerodynamic parameters such as CD and CL were compared for both cases with and without flaps. Figure 24 shows that using the k-omega SST turbulence model agreed well with the experimental results at a wind angle of attack of 0 degrees. This comparison validates the primary schemes and analysis parameters used in the simulations, ensuring their reliability.

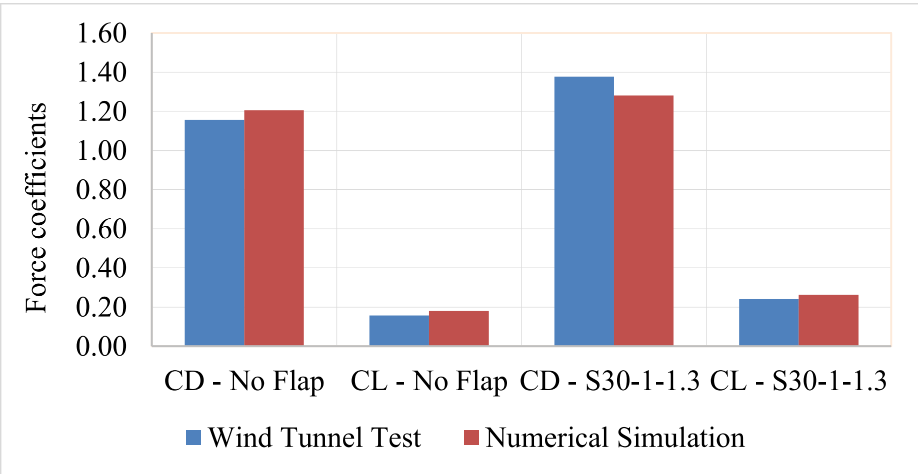

Figure 24. Aerodynamic coefficients of No-Flap case and S30-1-1.3 case.

4.4. Numerical analysis
This section discusses how flaps can suppress vortex-induced vibrations in the wind flow. The focus is on examining the aerodynamic characteristics of different flap geometries to understand how they affect wind flow behavior. The impact of flap countermeasure on the wind flow characteristics is assessed by analyzing many metrics, such as the power spectral density (PSD) of lift force, the flow structures, the root mean square (RMS) of pressure coefficient across the sectional perimeter, and the RMS of force coefficients.

4.4.1. Lift force. CFD analysis is conducted to reproduce the results obtained from experiments. The simulations correlate well with the experimental data, particularly in the unsteady lift force. Specifically, the lift force's power spectral density (PSD) exhibits a similar pattern to the vertical amplitude measured in the WTT. Figures 25 and 26 demonstrate that the power spectral density (PSD) attains its maximum value in the section without a flap and declines in the bridge girder where a flap is mounted.

As shown in Figure 27, the RMS lift force performs similarly. The girder without flaps has the maximum RMS of lift force, while the girder in the presence of flaps significantly drops around 60%.

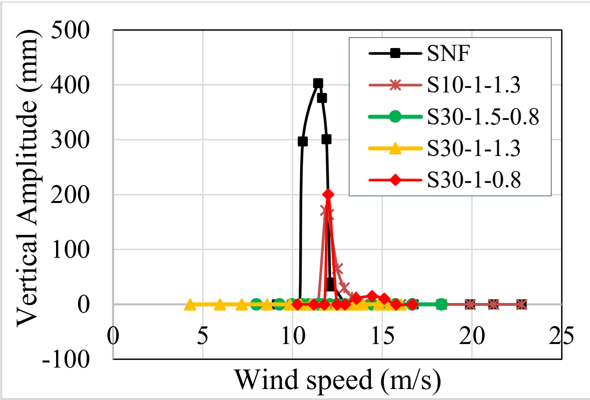

Figure 25. Vertical amplitude in WTT.

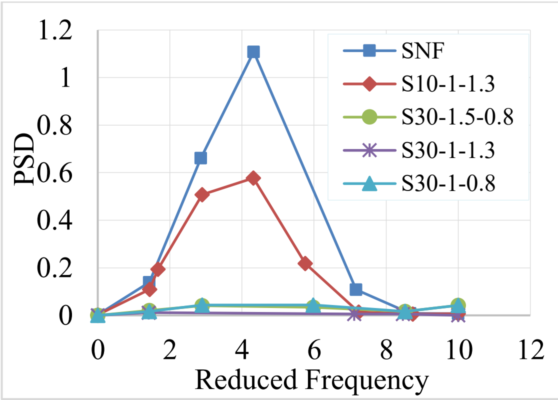

Figure 26. PSD of lift forces.

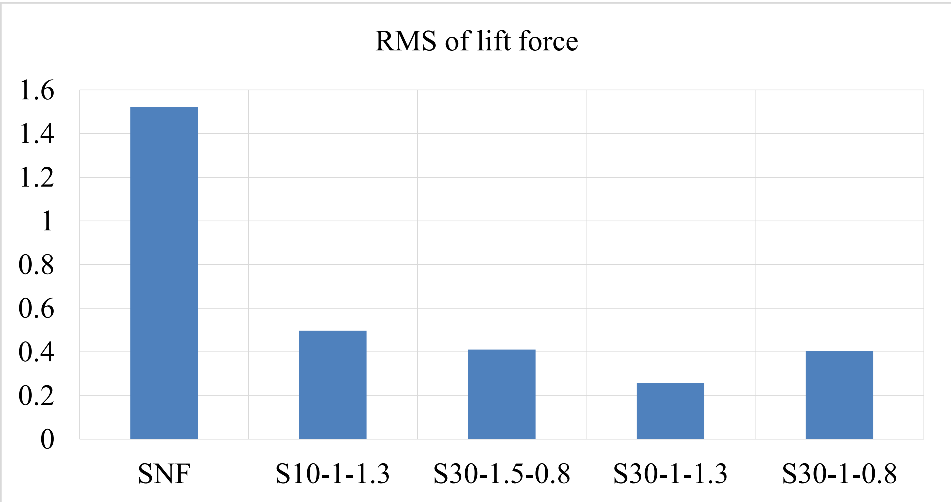

Figure 27. RMS of Lift Force.

4.4.2. RMS of pressure coefficient along the perimeter of bridge girder section. The pressure coefficient's RMS (root-mean-square) value exhibits similar behavior to the lift force. The RMS value is determined in numerical simulations by collecting the pressure coefficient's time history from various locations around the bridge girder section's perimeter. It is calculated as the root square of the sum of the squares of the coefficient of pressure fluctuation. The distribution of the root-mean-square (RMS) values for pressure coefficients around the bridge girder section is computed and shown in Figure 28. In Figure 28, it is shown that having an appropriate flap is crucial for minimizing the variation of pressure coefficient on a surface; as the angle of the flaps increases towards 30 degrees, the RMS value decreases. Figure 28 shows that the root-mean-square of pressure coefficients on the upper surface of a bridge girder is higher when no flaps are present. However, the pressure coefficients RMS underneath the girder are the same regardless of the angle of the flaps.

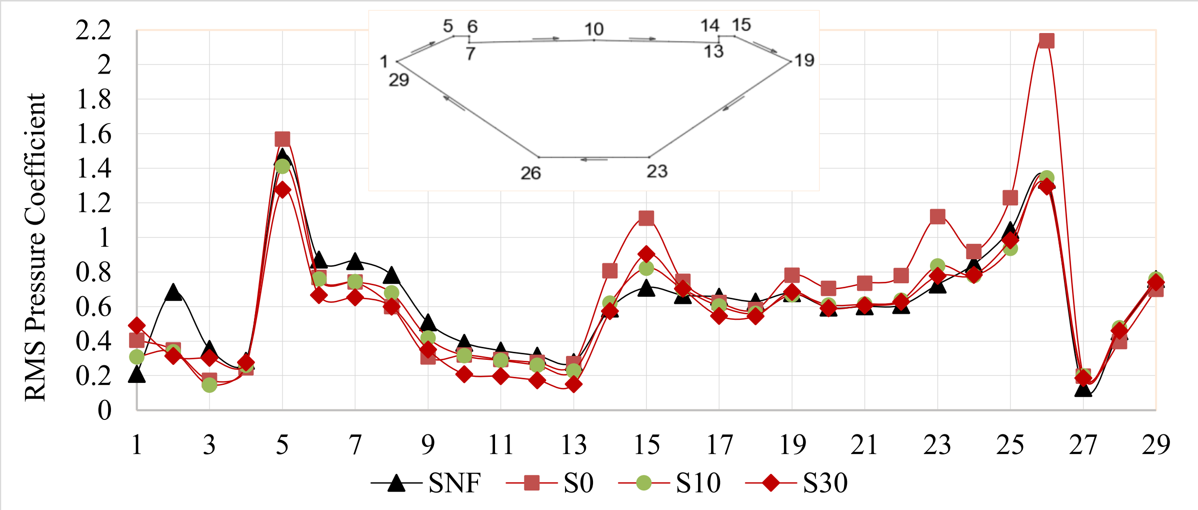

Figure 28. RMS of surface pressure coefficients.

4.4.3. Wind profile above the bridge girder. This section presents an analysis of turbulent intensity at various points ranging from the deck's surface to an elevation of approximately 10 meters. The results of this investigation are presented in Figure 29.

The investigation observed a significant difference in the turbulent intensity values between the girder portion without flaps and the portion with flaps at elevations above 6 meters. However, it exhibits substantial fluctuations at lower heights.

This study observed a significant increase in turbulent intensity when a flap was attached to the section, compared to the section without a flap. The study's findings indicate that the highest turbulence intensity level is evident when flaps are present, specifically when the flaps are at a 30-degree angle, as shown in Figure 29. Introducing a flap to the structure can cause disruptions to the wind profile in a particular area. The study identified that vigorous turbulent intensity occurs in the upper region of the section's surface.

4.5. Forced vibration test

Forced vibration tests were conducted using a CFD technique to determine the flutter derivatives of bridge girders with and without flaps. The simulation utilized a k-ω shear stress transport (SST) model, and dynamic mesh smoothing and re-meshing techniques were implemented. A user-defined function (UDF) defined the vertical 1DOF sinusoidal vibration parameters.

In accordance with the process outlined in Section 3, the flutter derivatives were determined using Equation (11) while maintaining a constant vibration frequency of 2.7 Hz and a translation amplitude of 0.003 m in the vibration test. A positive value for the flutter derivative H_1^* implies that the aerodynamic damping is negative. This is because the flutter derivative H_1^* depicts the aeroelastic transfer function between the wind force and the object displacement.

Two cases were considered in the dynamic numerical simulations: the No-Flap case and the S30-1-1.3 case, which involved a flap angle of 30 degrees, a flap length of 1m, and a gap of 1.3m. Figure 30 illustrates the time-dependent behavior of the lift force, which was recorded for each scenario to elucidate the vertical Vortex-Induced Vibration. The flutter derivative H_1^* was calculated using Equation (11), and four reduced velocities (1, 2, 3, and 5) were considered for each harmonic motion.

The Wind Tunnel Test (WTT) revealed that vortex-induced vibration occurred at a reduced velocity of 2. Figure 30 shows that at the reduced velocity of 2, the flutter derivative H_1^* was positive for the section without a flap, which coincided with the region where the highest amplitude of Vortex-Induced Vibration was observed during the Wind Tunnel Test. Conversely, the flutter derivative had different negative values in cases where a flap was installed on the section.

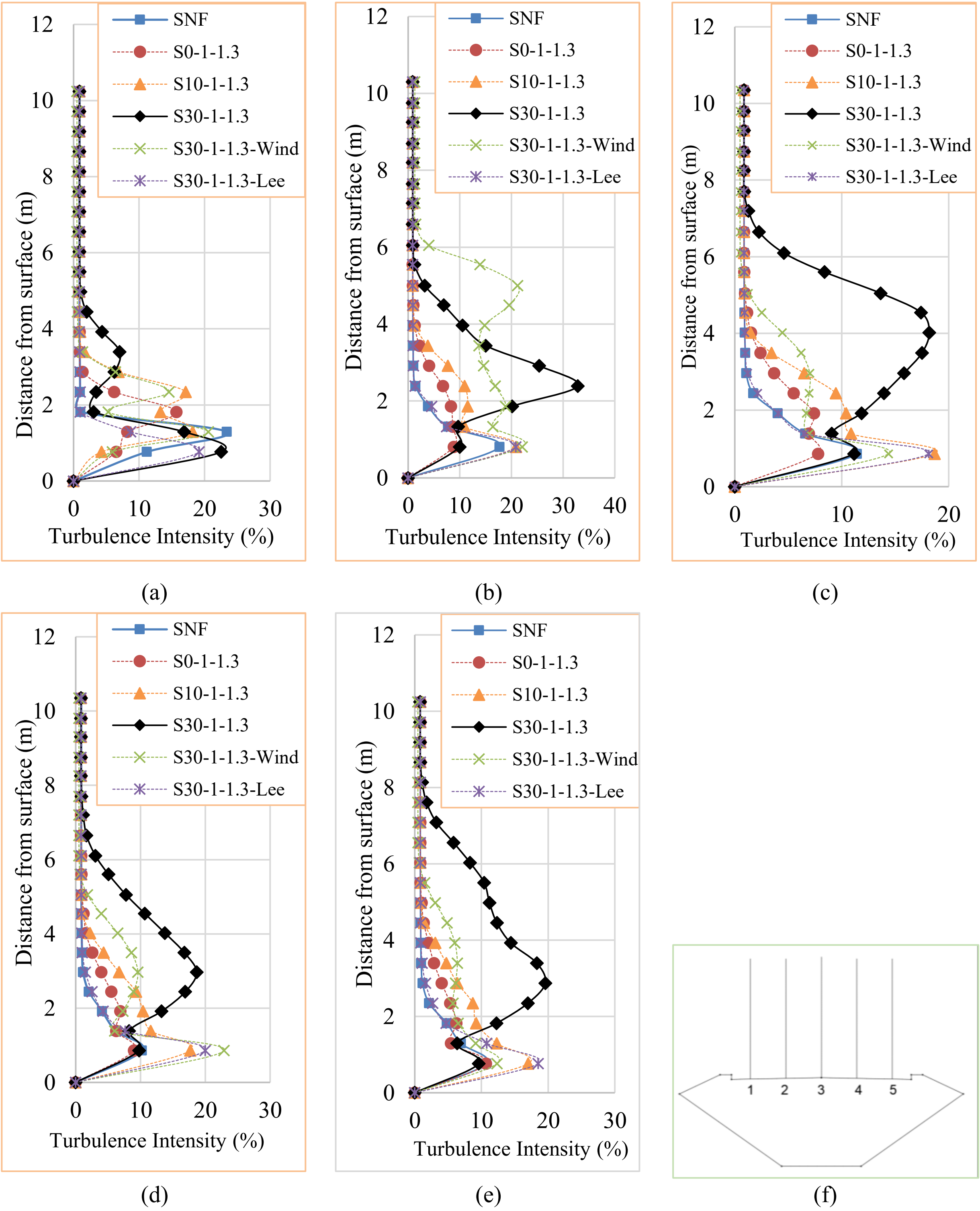

Figure 29. Turbulent intensity: (a) Position 1, (b) Position 2, (c) Position 3, (d) Position 4, (e) Position 5, (f) Observation positions.

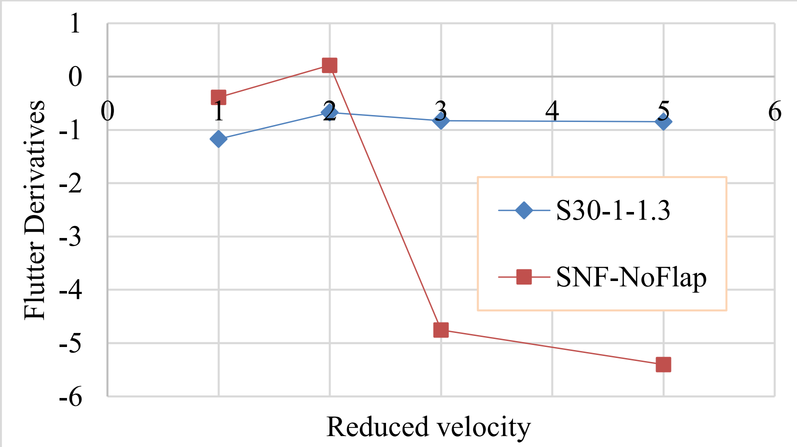

Figure 30. Flutter derivatives H_1^*.

5. Conclusions

Wind tunnel tests and CFD simulations are carried out to analyze the proposed stabilizing mechanisms of flap countermeasures for motion-induced vortex vibration of the bridge girder section. The study examines the aerodynamic instability of the bridge girder in the presence of aerodynamic countermeasures, focusing on the flap's stabilizing mechanism. The results of this study provide valuable insights into the altered flow characteristics around the bridge section in the presence of the flap countermeasure, leading to reduced vibration amplitude. The conclusions are as follows:

- The flap countermeasure has proved to be helpful in the bridge-girder system. The wind tunnel testing results on a section of the bridge girder are detailed, demonstrating that the VIV has increased in both the vertical and torsional directions.
- Changing flap configurations is beneficial in most cases. The research findings suggest that the efficiency of the flap countermeasure is highly dependent on its installed location and length. Therefore, the flap with a 30-degree angle and a large gap was the most effective at mitigating vibration.
- Particle Image Velocimetry (PIV) measurements were executed to clarify and comprehend the changes in flow structures around the bridge girder and at the leeward side of the section.
- CFD simulation is introduced to reproduce the VIV process of the bridge girder section. The RANS method that uses the k-omega SST turbulence model in a two-dimensional computational domain is examined. The results show acceptable accuracy, laying the foundations for the following investigations.
- Flutter derivatives help to understand the VIV of bridge deck sections and provide insights into the mechanism behind the flap countermeasure's effectiveness in mitigating the VIV amplitude of the box girder.

From the efforts above, the potential general control effect of the aerodynamic measures in similar hexagonal box girders can be attractive.

References

[1] Yozo F, Dionysius S 2013 Vibration Mechanisms and Controls of Long-Span Bridges: A Review *Structural Engineering International* **23(3)** 248–268
[2] Yozo F, Kichiro K, Hiroshi T 2012 *Wind Resistant Design of Bridges in Japan* (Springer)
[3] Fujino Y, Yoshida Y 2002 Wind-induced vibration, and control of Trans-Tokyo Bay Crossing Bridge *Journal of Structural Engineering* **128** 1012-1025

[4] Katsuchi H, Yamada H, Etoh K, Nagai S, Sekiguchi T, Morikawa Y, Nakagaki T, and Yui R 2013 Vortex-induced vibration, and its countermeasures observed at the long-span cable-stayed bridge *Proceedings of 12th America Conference on Wind Engineering* (No.12.2 Seattle USA)
[5] Li H, Laima S, Zhang Q, Li N, Liu Z 2014b Field monitoring and validation of vortex-induced vibrations of a long-span suspension bridge *Journal Wind Engineering and Industrial Aerodynamic* **124** 54–67
[6] Laima S, Li H, Chen W, Ou J, 2018b Effects of attachments on aerodynamic characteristics and vortex-induced vibration of twin-box girder *Fluids Structure* **77** 115–133
[7] Yongxin Yang, Rui Zhou, Yaojun Ge, Yanliang Du, and Lihai Zhang 2018 Sensitivity Analysis of Geometrical Parameters on the Aerodynamic Performance of Closed-Box Girder Bridges *Sensors* **18(7)** 2053
[8] Dat Anh Tran, Hiroshi Katsuchi, Hitoshi Yamada, Mayuko Nishio 2014 Numerical analysis for the flap on wind flow across box girder section *Journal of Structural Engineering* 60A 387-396
[9] Ferziger JH, Peric M 2002 *Computational Methods for Fluid Dynamics* (Springer)
[10] Shimada K, Ishihara T 1999 Prediction of aeroelastic vibration of rectangular cylinders by model *Journal of Aerospace Engineering* **12** 122-135
[11] FR Menter 1994 Two-equation eddy-viscosity turbulence models for engineering applications *AIAA Journal* **32(8)** 1598-1605
[12] Simiu E, Scanlan RH 1996 *Wind Effects on Structures* (John Wiley & Sons)
[13] JD Anderson, JR 1995 *Computational Fluid Dynamics: The basics with applications* (McGraw Hill)
[14] HK Versteeg, W Malalasekera 2007 *An introduction to Computational Fluid Dynamics – The Finite Volume Method* (Pearson)
[15] Sarwar MW, Ishihara T 2010 Numerical study on suppression of vortex-induced vibrations of box girder bridge section by aerodynamic countermeasures *Journal of Wind Engineering and Industrial Aerodynamics* **98** 701-711
[16] Lee S, Lee JS, Kim JD 1997 Prediction of vortex-induced wind loading on long-span bridges *Journal of Wind Energy and Industrial Aerodynamics* **67-68** 267-278
[17] Brusiani F, Miranda S, Patruno L, Ubertini F, Vaona P 2013 On the evaluation of bridge deck flutter derivatives using RANS turbulence models *Journal of Wind Engineering and Industrial Aerodynamics* **119** 39-47
[18] Watanabe S, Fumoto K 2008 Aerodynamic study of slotted box girder using computational fluid dynamics *Journal of Wind Engineering and Industrial Aerodynamics* **96** 1885-1894
[19] Francesco R, Enrico T, Horia H 2002 Pressure Distribution, Aerodynamic Forces and Dynamic Response of Box Bridge Sections *Journal of Wind Engineering and Industrial Aerodynamics* **90** 1135-1150
[20] Farquharson FB Aerodynamics Stability of Suspension Bridges with Special Reference to the Tacoma Narrows Bridge. Parts I, III, and IV (Bulletin University of Washington Engineering Experiment Station, Seattle, WA, USA) **116** 1949–1954